

GROUND SIGNATURE EXTRAPOLATION OF THREE-DIMENSIONAL NEAR-FIELD CFD PREDICTIONS FOR SEVERAL HSCT CONFIGURATIONS

M.J. Siclari
Grumman Corporate Research Center
Bethpage, New York 11714

SUMMARY

A CFD analysis of the near-field sonic boom environment of several low boom High Speed Civilian Transport (HSCT) concepts is presented. The CFD method utilizes a multi-block Euler marching code within the context of an innovative mesh topology that allows for the resolution of shock waves several body lengths from the aircraft. Three-dimensional pressure footprints at one body length below three-different low boom aircraft concepts are presented. Models of two concepts designed by NASA to cruise at Mach 2 and Mach 3 were built and tested in the wind tunnel. The third concept was designed by Boeing to cruise at Mach 1.7. Centerline and sideline samples of these footprints are then extrapolated to the ground using a linear waveform parameter method to estimate the ground signatures or sonic boom ground overpressure levels. The Mach 2 concept achieved its centerline design signature but indicated higher sideline booms due to the outboard wing crank of the configuration.

Nacelles are also included on two of NASA's low boom concepts. Computations are carried out for both flow-through nacelles and nacelles with engine exhaust simulation. The flow-through nacelles with the assumption of zero spillage and zero inlet lip radius showed very little effect on the sonic boom signatures. On the other hand, it was shown that the engine exhaust plumes can have an effect on the levels of overpressure reaching the ground depending on the engine operating conditions. The results of this study indicate that engine integration into a low boom design should be given some attention.

INTRODUCTION

Because of a renewed interest in the deployment of a fleet of High Speed Civilian Transports (HSCTs) during the first decade of the 21st century, NASA and industry are devoting a considerable amount of effort to the study of sonic booms that accompany supersonic flight. One of the priority economic issues in the development of such a fleet is whether overland flight is possible. Overland supersonic flight might significantly increase the profitability of a fleet of supersonic transports. NASA's High Speed Research Program is devoting a major effort to the area of sonic boom prediction.

Currently, efforts have focused on the use of careful area shaping to design low boom concepts. Computer codes currently in use for the design and analysis of low boom configurations are based on Whitham's modified linear theory analysis (Ref. 1), which was extended to apply to lifting bodies by Walkden (Ref. 2).

Since the first interest in supersonic transports in the early '70's, computers and computational capabilities have increased by orders of magnitude. Presently, computational fluid dynamics (CFD) codes can compute the complete nonlinear flow about an aircraft in minutes to an hour on a supercomputer.

This paper describes the use of a supersonic marching CFD methodology to predict the near-field three-dimensional pressure patterns generated by candidate low boom designs. A very efficient three-dimensional Euler finite volume code is used for these predictions. Calculations were carried out using a grid topology that has been modified to reduce the inaccuracies caused by grid spreading often suffered with CFD methods when calculations several body lengths downstream become necessary.

Each aircraft design generates a unique pressure footprint much like a fingerprint. The present approach is to use the CFD code to predict the pressure footprint typically at one or more body lengths below the aircraft. At this distance, the flow disturbances will have become small enough such that a method based on linear theory will be valid and allow the extrapolation of this footprint to the ground.

In carrying out this procedure several issues still remain. It is still not clear how far from the aircraft to carry the computation so that linear theory will apply. There may not be any hard and fast rules in that the distance may be governed by several parameters such as Mach number and surface slopes. In Ref. 3, the computations were carried out to one, two, and three body lengths below the aircraft. These signatures were then extrapolated to the ground using the code of Thomas (Ref. 4), which uses a waveform parameter method for the extrapolation. The resulting signatures showed no significant differences in the level of the sonic boom although the shapes of the signatures showed some minor differences. Whether these minor differences are due to varying accuracy in the computations, or to three-dimensional effects of the flow field, is still not well understood. The one-dimensional extrapolation of these signatures naturally neglects all three-dimensional effects, and hence it is important that these effects be diminished prior to using an extrapolation theory to the ground. As a result of the findings in Ref. 3, all of the computations presented in this paper were carried out to one body length below the aircraft.

FEATURES OF CFD METHOD FOR SONIC BOOM COMPUTATIONS

The present CFD method has been developed in the last several years by the author and is described in detail in Refs. 5 and 6. The technique involves solving the unsteady three-dimensional Euler equations in a spherical coordinate system using a central difference crossflow finite volume scheme within the context of an implicit marching technique. The equations are driven to a steady state solution at each marching plane using a multi-stage Runge-Kutta time integration scheme with local time stepping, residual smoothing, and multi-grid to accelerate convergence. The implicit nature of the marching scheme removes constraints in the axial step size other than those required for geometric accuracy. The scheme is very fast and requires little memory, and hence computations on grids with a large number of points can be carried out quite easily. The computation is started by assuming a small conical nose based on the true geometric nose cross section of the vehicle. All shocks are currently captured within the context of this scheme.

Standard aerodynamic CFD computations are primarily concerned with the accurate prediction of the surface characteristics of the aircraft and, at most, the behavior of the flow field in the immediate vicinity of the aircraft. Sonic boom computations, on the other hand, require the resolution of the aircraft flow field, in particular, the shock wave pattern several body lengths downstream. For example, to predict the pressure footprint at just one body length below the aircraft, the computation must be carried out to three to five body lengths aft of the aircraft depending upon the freestream Mach number. The entire computation, for supersonic flows, is bounded by the bow shock generated by the nose of the aircraft. The distance between the bow shock and vehicle surface increases as a function of the axial distance from the nose of the vehicle. Given a fixed number of mesh points between the bow shock and inner boundary, this results in

poor resolution of the shock waves. There are several possible approaches to alleviate this problem. One is to increase the number of grid points in areas of the computation far from the nose of the vehicle and use a unique mesh stretching or adaptation that puts grid points in areas where they are most needed to resolve the shocks.

In this paper, a different approach is adopted that relies upon knowledge of the behavior of the flow field and does not require hundreds of points between the outer bow shock and the inner boundary. Figure 1 illustrates the basic features of this scheme. The computation is carried out in the context of an axial multi-block scheme. The meshes of the block interfaces need not match. This allows for an increase in mesh points as the grid gets further from the nose of the vehicle. It also allows for discontinuities in geometry at grid interfaces to simulate inlets and exhaust flows. At the outer boundary, the mesh is adapted to the bow or outermost shock wave. This also conserves grid points. The outer boundary is self-adapted as the computation proceeds downstream. A difference in just one or two degrees at the outer boundary can cause a significant loss in grid points outside the bow shock and, hence, a corresponding loss in resolution. To avoid the large distance between the bow shock and inner boundary downstream of the aircraft, the inner boundary is modeled as a rotated Mach cone surface downstream of the sting or afterbody extension of the aircraft. The length of the sting will then dictate how far the computation can proceed downstream of the aircraft since the sting will eventually affect the recompression shock of the aircraft's signature. To achieve a signature one body length below the aircraft, the length of the sting will typically be one-half to one aircraft length long.

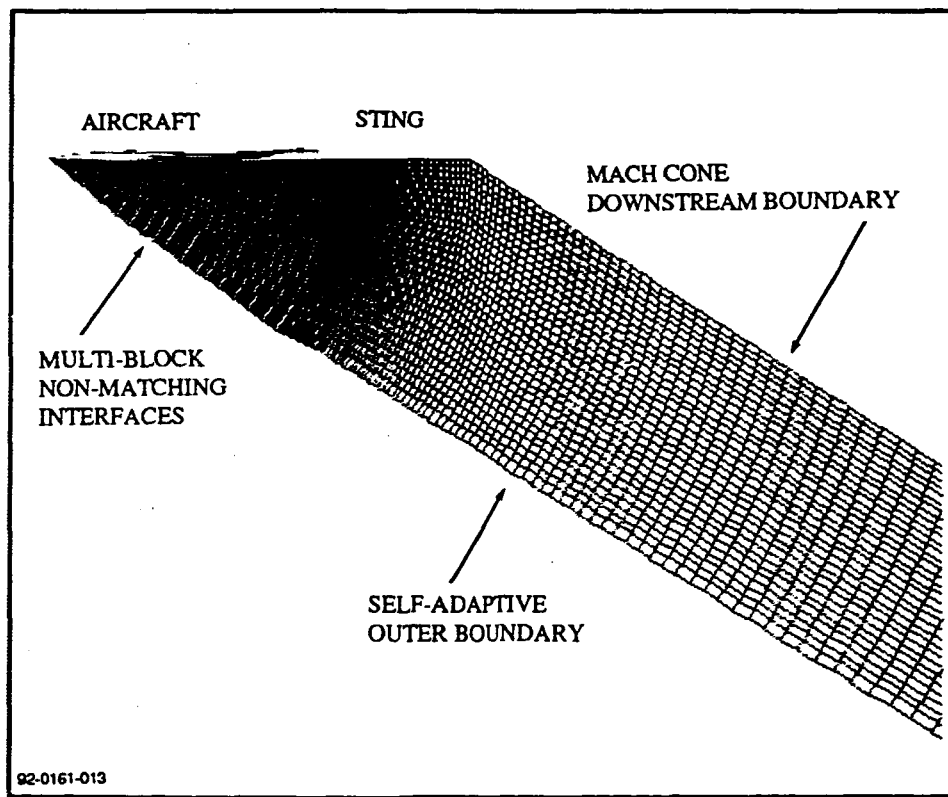


Figure 1. Grid topology and features used for sonic boom computations.

NASA'S LOW BOOM MACH 2 AND MACH 3 CONCEPTS

In Ref. 3, the signatures of NASA's Mach 2 and Mach 3 concepts without engine nacelles were computed using the present approach. Some details of the design of the wind tunnel models for these two concepts are presented in Ref. 7. Wind tunnel models of these two concepts were also built and tested. Both aircraft were designed to be about 300 feet in length. The wind tunnel models were built to 1/300th scale, making them about one foot in length. Figure 2 shows a comparison between wind tunnel data and computed signatures at one body length below the aircraft. Good correlation was achieved for the forward part of the signature. The latter half of the measured wind tunnel signature exhibited two additional secondary shocks and a larger expansion in comparison to the computed results. The origin of these secondary shocks is still being studied.

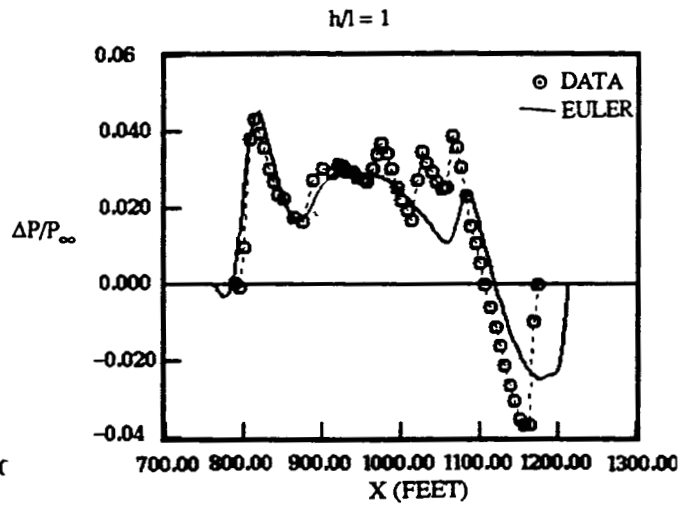
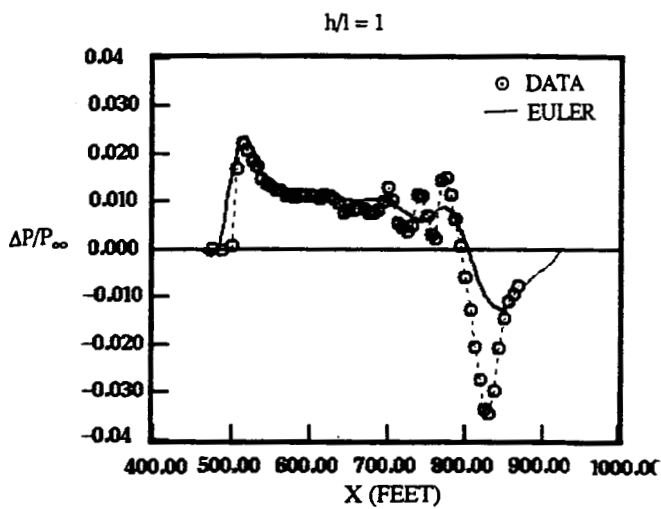
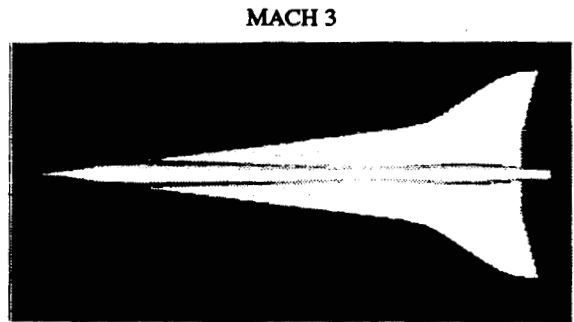
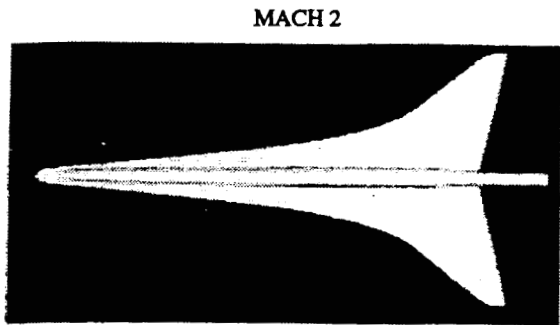
Both the computed and measured signatures were extrapolated to the ground using the code of Thomas (Ref. 4). Figure 3 shows a comparison of these results. The Mach 2 concept was designed to cruise at an altitude of 55,000 feet and the Mach 3 concept at 65,000 feet. For both concepts, the extrapolated ground signatures from both the computation and wind tunnel data compared favorably. In the present study, a reflection factor of 1.9 was used in computing the extrapolated ground signatures. Also noted on the figures is the target design signatures for both concepts. The Mach 2 aircraft compared favorably with its intended target signature, whereas the extrapolated signature of the Mach 3 aircraft was well above its design target levels. The two concepts were designed for two different types of signatures: the Mach 2, for a flat topped or constant level signature prior to expansion, and the Mach 3, for a ramped signature. The discrepancy in design signature and extrapolated wind tunnel data and computation for the Mach 3 concept may possibly be attributed to the breakdown of linear theory at the higher Mach number and also possibly due to the inability of being able to achieve the ramped type of signature.

THE BOEING-911 LOW BOOM MACH 1.7 CONCEPT

Figure 4 shows the geometry of the Boeing-911 low boom Mach 1.7 concept. Also shown are the computed signature at one body length and the extrapolated ground signature for the aircraft at an altitude of 44,000 feet. This signature exhibits three shocks prior to the expansion. The first shock is the nose shock and the second is the wing shock. The third shock prior to the expansion is most likely the sting shock. The fuselage geometry was truncated for the computation and fitted with a sting. The interesting aspect of this concept is that the character of the signature persists to the ground with very little coalescence of these shocks, at least according to the waveform parameter method used for the extrapolation. The Mach 3 concept indicated a higher degree of coalescence to an N-wave. The Boeing-911 concept based on the present computations indicates about a 1.5 lbs/ft² overpressure.

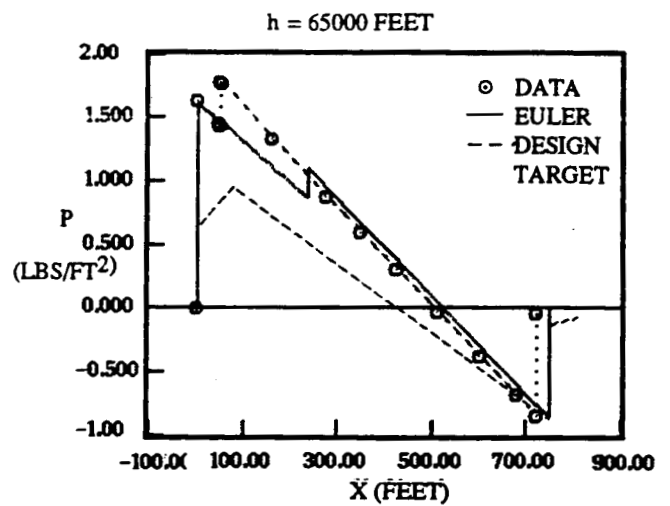
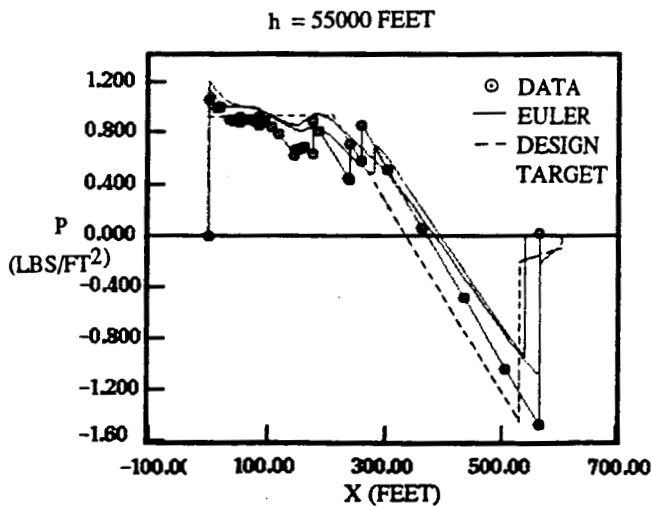
Figure 5 shows some illustrations of the computed surface pressures for this concept along with some pressure contours just aft of the configuration.

Figure 6 shows the three-dimensional pressure footprint of the aircraft in a plane one body length below the aircraft. Also shown are the centerline sampling and sideline signatures of the footprint. The double shock character of the centerline signature persists laterally. The third sting shock is localized to the vicinity of the centerline. Also, the highest signature overpressures are localized near the centerline and attenuate laterally. As will be shown in a subsequent section, the lateral and monotonic attenuation of signature overpressures is not always the case.



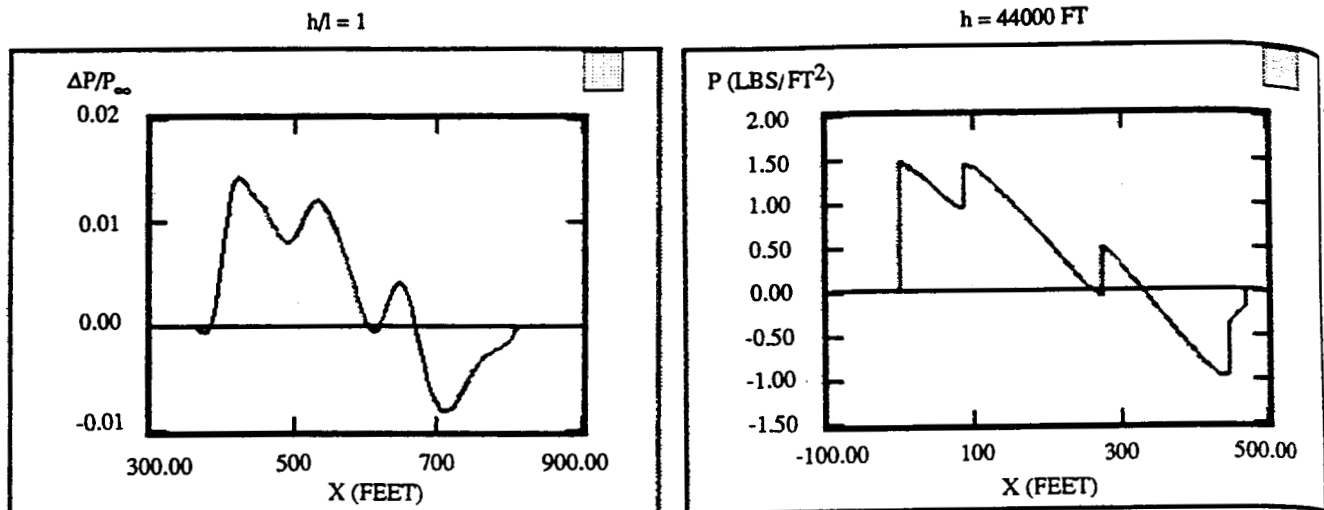
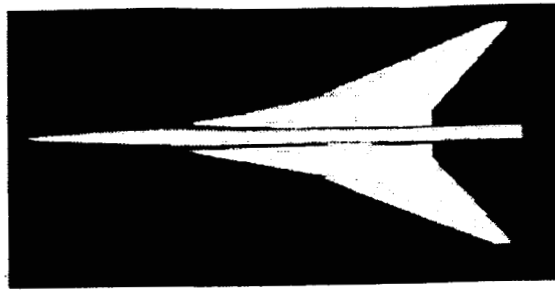
92-0161-014

Figure 2. Comparison of computed and wind tunnel pressure signatures at $h/l=1$ for NASA's Mach 2 and Mach 3 low boom configurations.



92-0161-015

Figure 3. Comparison of extrapolated ground signatures from computations and wind tunnel data at $h/l=1$ for the Mach 2 and Mach 3 aircraft.



92-0161-001

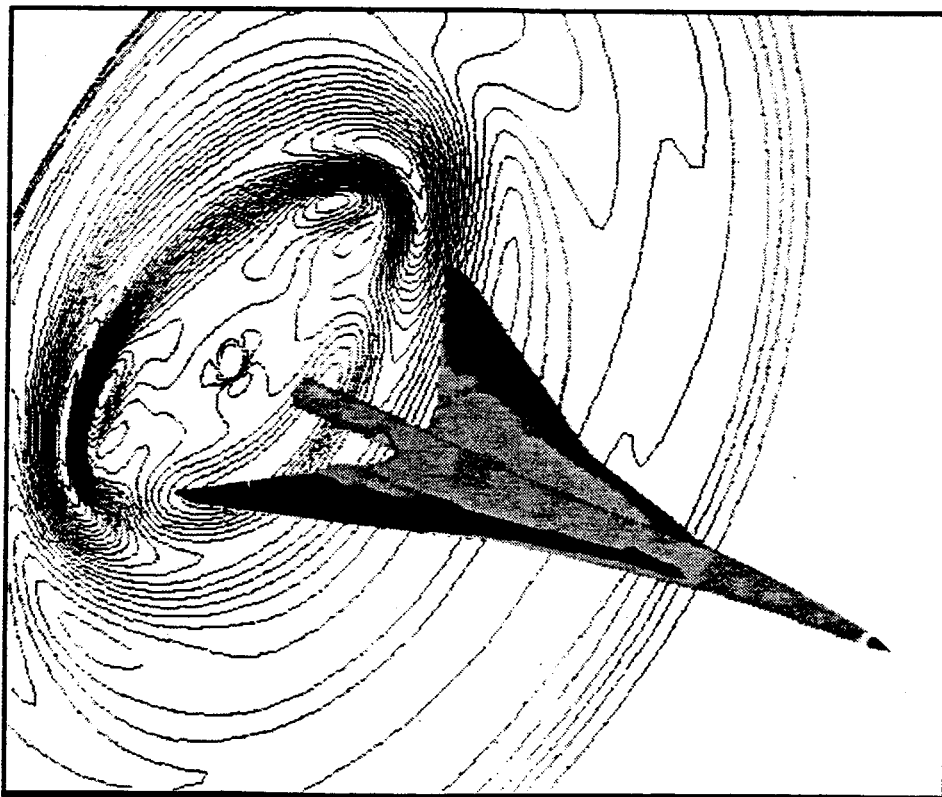
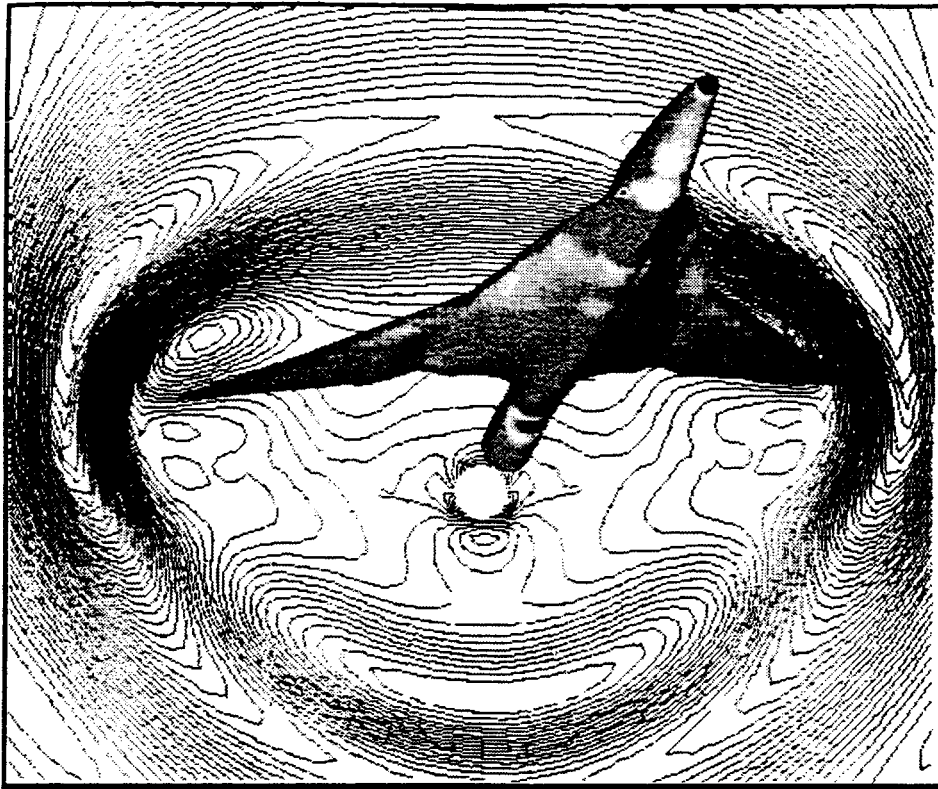
Figure 4. Computed and extrapolated ground signatures for the Boeing-911 Mach 1.7 low boom configuration.

THE MACH 2 AND MACH 3 CONCEPTS WITH FLOW-THROUGH NACELLES

Extending the study of Ref. 3 to include the effects of nacelles was the primary thrust of the present study. Figure 7 shows the Mach 2 and Mach 3 geometry with the original designed nacelle geometry used in the present computations. The nacelle geometry was the same for both configurations. The locations of the nacelles were different; with the Mach 2 aircraft having the nacelles situated more closely to the underside of the aircraft. The nacelles were not staggered in the present study for computational convenience. The nacelles were basically axisymmetric. The first set of computations carried out was for flow-through nacelles. The computation assumed that all of the mass entering the face of the nacelles or inlet was completely swallowed. The exhaust assumed freestream and axial flow conditions.

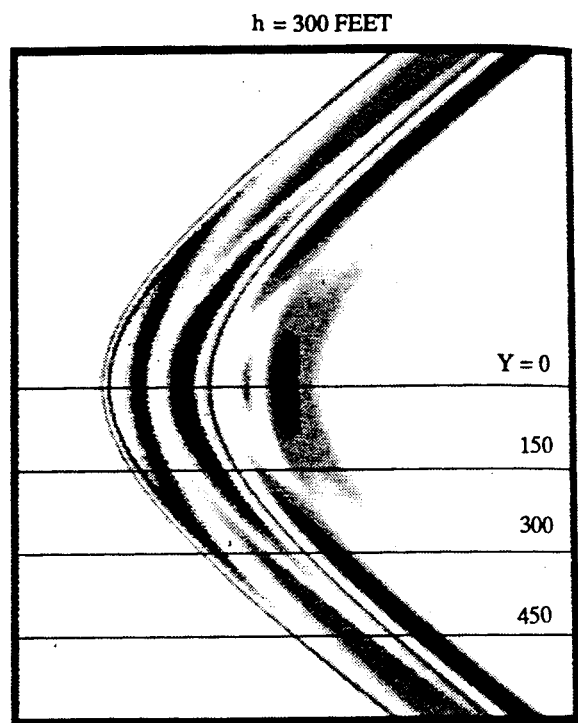
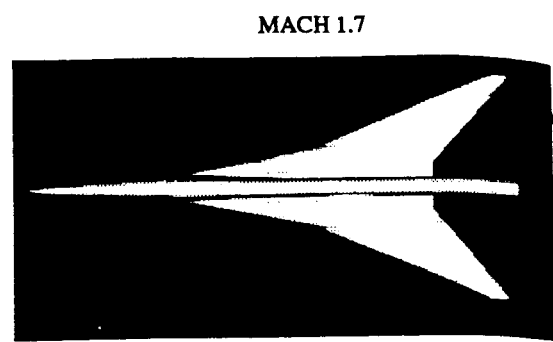
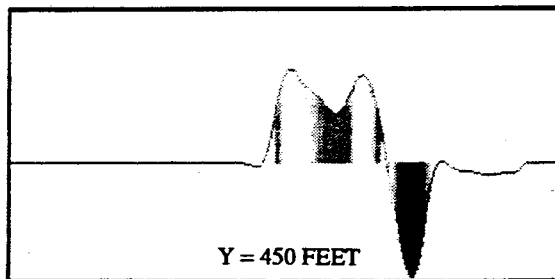
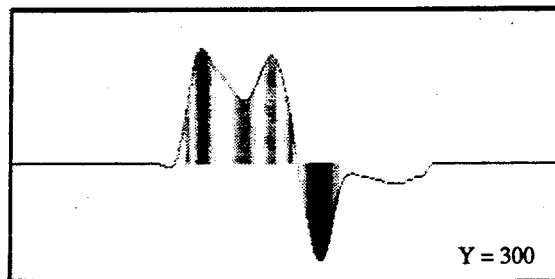
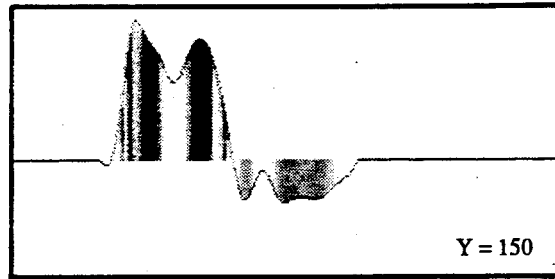
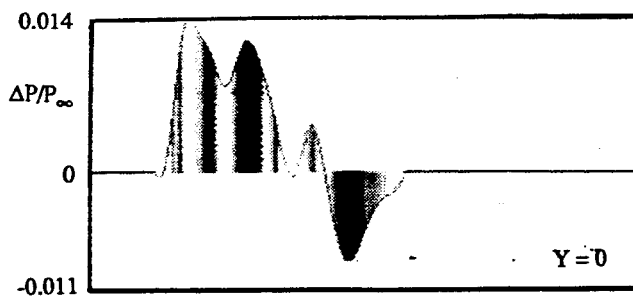
Figure 8 shows the pressure footprint computed with flow-through nacelles at one body length below the aircraft for the Mach 2 concept. The flow-through nacelles have only a minor effect on the pressure footprint and signatures in comparison to those computed in Ref. 3 without nacelles. Figure 8 also shows that the sideline signatures exhibit a higher overpressure than the centerline signature. This was found to be true in Ref. 3 and is caused by the outboard wing crank of the aircraft.

In a similar fashion, Figure 9 shows the pressure footprint for the Mach 3 concept. The flow-through nacelles on the Mach 3 aircraft also have only a minor effect on the signatures in



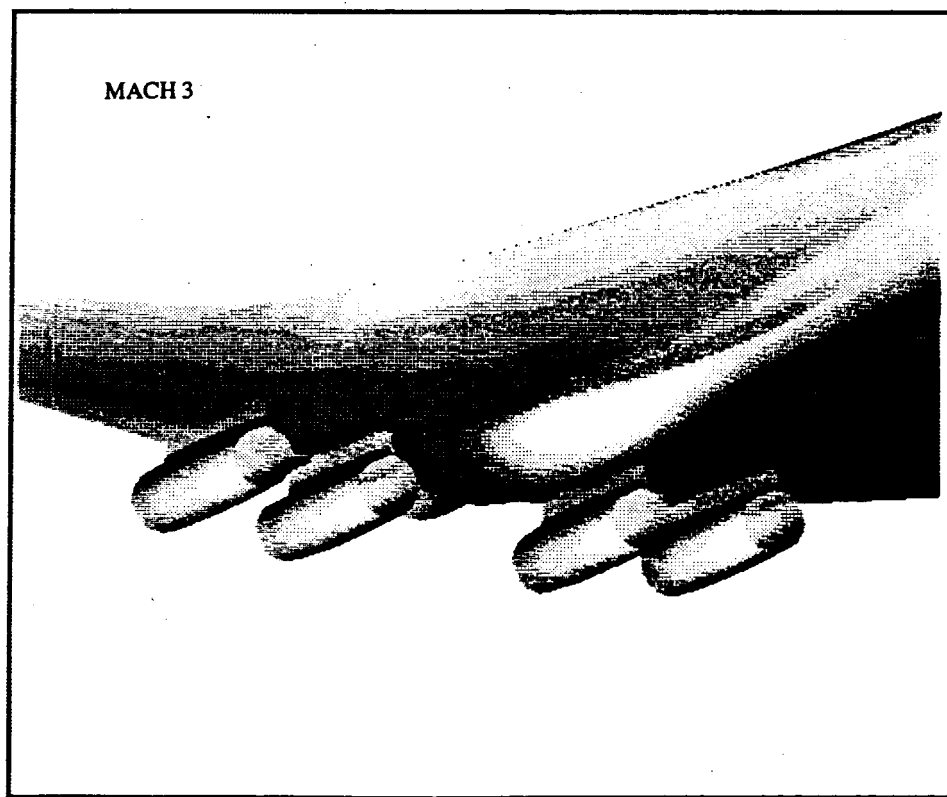
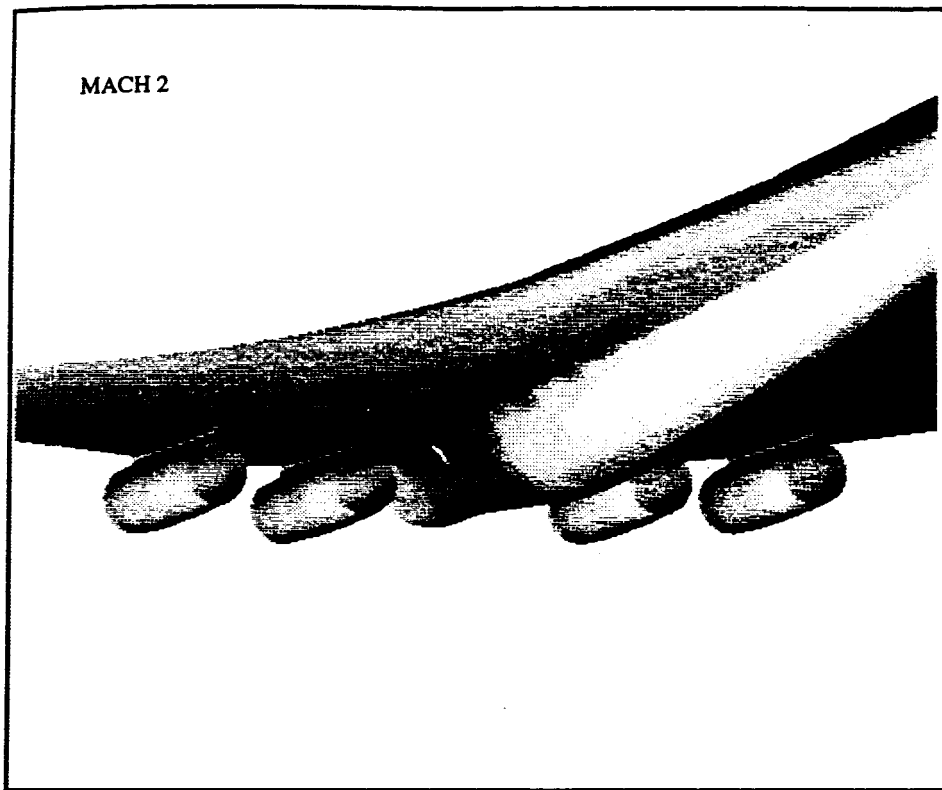
92-0161-011

Figure 5. Surface pressures and downstream pressure contours for the Boeing-911 Mach 1.7 low boom configuration.



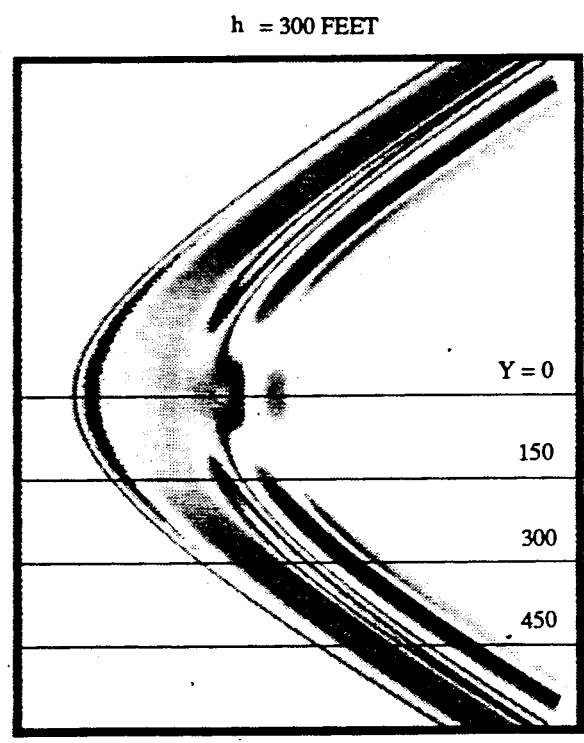
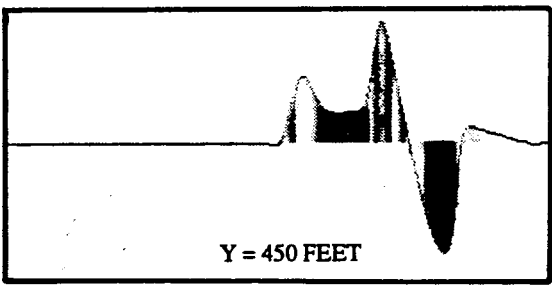
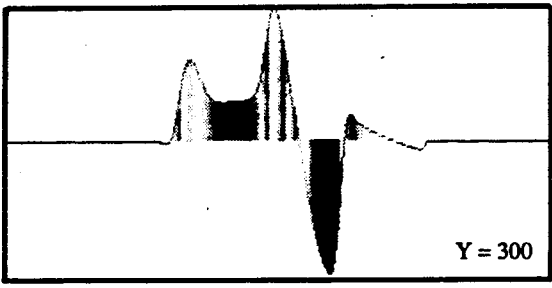
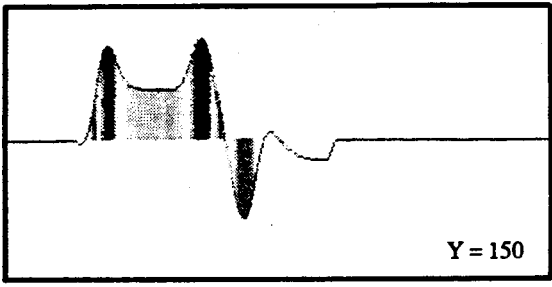
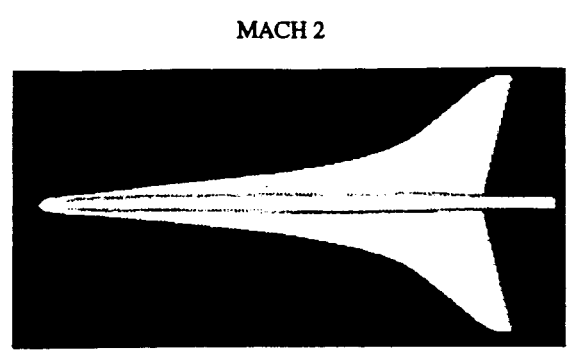
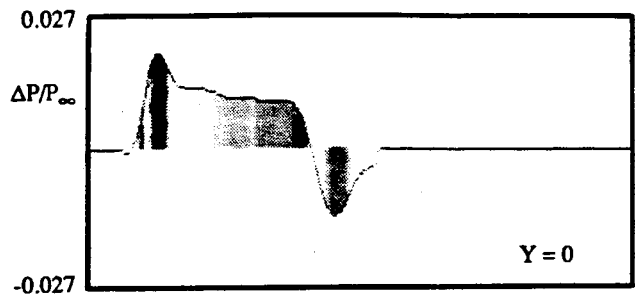
92-0161-017

Figure 6. Pressure footprint and sideline signatures at $h/l=1$ for the Boeing-911 Mach 1.7 low boom aircraft.



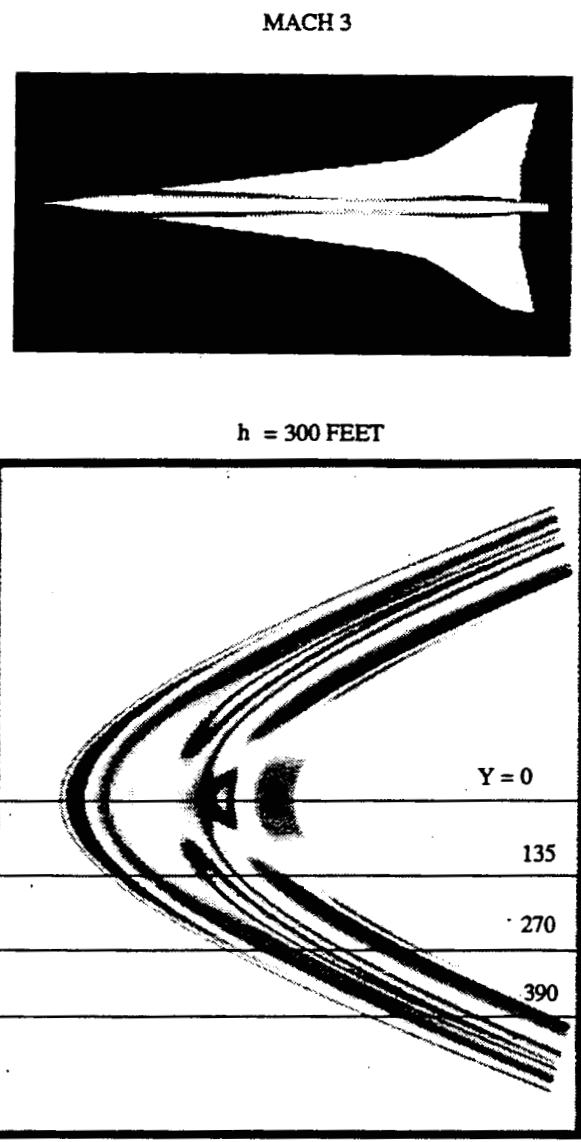
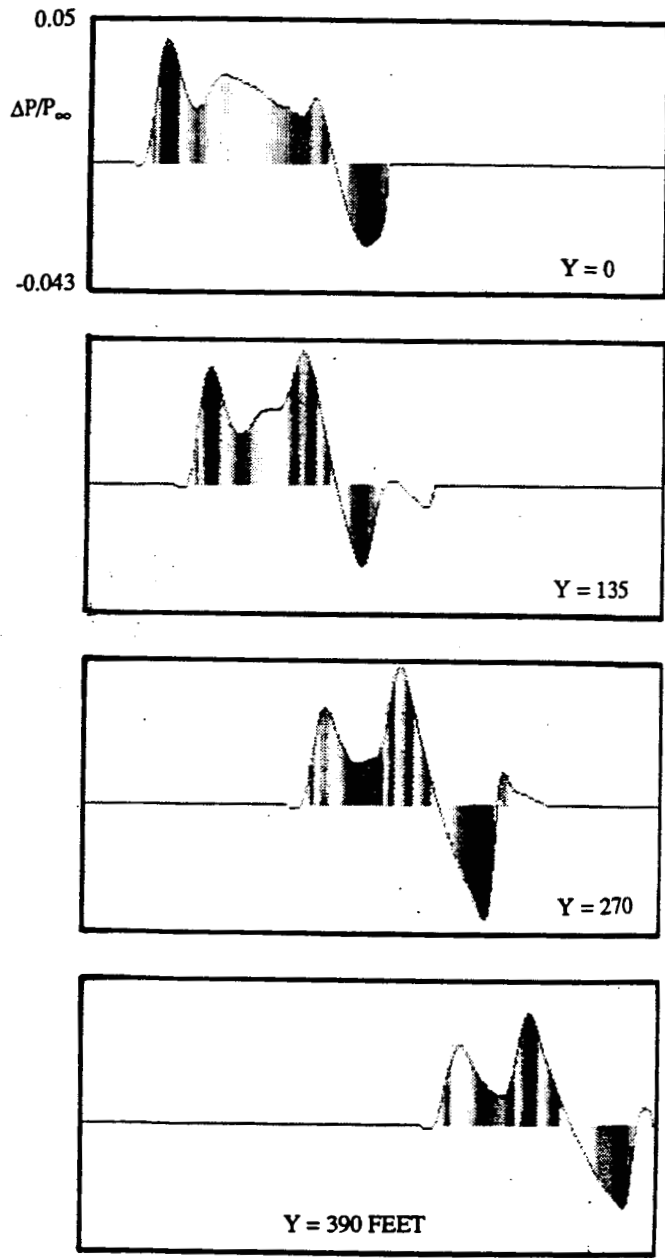
92-0161-012

Figure 7. Geometry of the NASA Mach 2 and Mach 3 low boom aircraft with four nacelles.



92-0161-018

Figure 8. Pressure footprint and sideline signatures at $h/l=1$ for the NASA Mach 2 low boom aircraft with flow-through nacelles.



92-0161-019

Figure 9. Pressure footprint and sideline signatures at $h/l=1$ for the NASA Mach 3 low boom aircraft with flow-through nacelles.

comparison with those computed in Ref. 3 without nacelles. As with the Mach 2 concept, the Mach 3 aircraft also indicates higher sideline overpressures due to the outboard crank of the wing.

Figure 10 serves to show the effect of the wing crank on the sideline or lateral attenuation of peak overpressures that was first computed in Ref. 3. One can take the sideline signatures of Figures 8 and 9 and, using the Thomas code, extrapolate the individual sideline signatures to the ground with the appropriate h/l and azimuthal angle computed from these figures. These extrapolations naturally assume that three-dimensional effects have diminished and can be neglected in the one-dimensional extrapolation. If one then takes the peak overpressure and plots them versus sideline or lateral distance in miles, Figure 10 results. For the Mach 2 concept, the sideline signatures exhibit two shocks prior to expansion. Both peak overpressures were plotted in Figure 10 for the Mach 2 aircraft. As indicated by this figure, larger overpressures occur in the sideline signatures of this aircraft. These larger sideline overpressures are primarily a three-dimensional effect due to the cranked outboard section of the wing, which may not be accounted for in the sonic boom minimization design theory. The same type of sideline overpressure plot is shown for the Mach 3 concept. The Mach 3 ground signatures exhibited primarily an N-wave type of behavior. Hence, only one peak sideline overpressure is plotted. Even so, slightly higher levels of overpressure are indicated off of the centerline trajectory of the vehicle.

Figure 10 can be very instructive in critiquing the design of a low boom aircraft. Both concepts have a greater than 1 lb/ft^2 corridor of 50 miles (i.e., ± 25 miles) approximately. Actually, the Mach 3 concept has a slightly smaller corridor, about 40 miles. The type of curves shown in Figure 10 could also be optimized to yield the smallest corridor of boom annoyance by designing a vehicle with the fastest lateral attenuation of maximum overpressure.

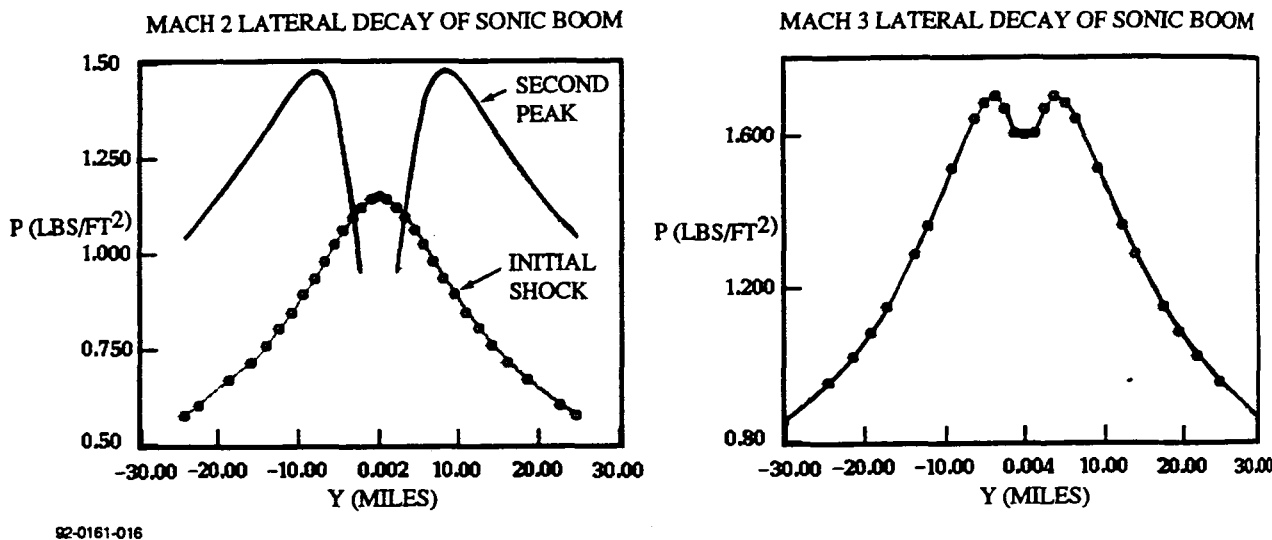


Figure 10. Sideline ground peak overpressure decay for NASA's Mach 2 and Mach 3 configurations without nacelles.

THE MACH 2 AND MACH 3 CONCEPTS WITH NACELLES AND EXHAUST SIMULATION

In this section, a detailed study of the effects of the nacelles including the engine exhaust simulation is presented, along with more details of the computations cited earlier with nacelles.

The computation was carried out on seven grid blocks containing the following:

<u>Block</u>	<u>Mesh</u>	<u>Grid Points</u>
1	41x37x11	6,687
2	49x47x24	55,272
3	69x57x21	82,593
4	79x75x38	225,150
5	143x109x11	171,457
6	113x119x21	282,387
7	113x109x85	<u>1,046,945</u>
		1,880,491 TOTAL

The mesh is described as (circumferential by normal by axial number) grid points. A total of 1.9 million grid points was used for the complete computation to yield the pressure field approximately one body length below the vehicle. The first four grid blocks served to gradually increase the number of grid points and switch from a simple body grid to a wing-body grid as the computation proceeded aft on the vehicle. The fifth grid block contained the engine nacelles and the special grid developed for their geometry. The sixth block reverted to a wing-body grid containing the engine exhaust. The nacelles extended beyond the wing trailing edge which complicated the boundary conditions. The seventh grid reverted to a simple polar grid since the wing no longer existed, only the sting and engine exhausts. The engine exhausts persisted in the grid until the exhaust was extrapolated out of the grid when it intersected with the downstream Mach cone surface. The entire computation took approximately one hour on a Cray YMP computer.

As mentioned earlier, the inlets were initiated by assuming that all of the mass entering the face of the engine is swallowed or zero spillage is assumed. The exhaust of each nacelle was simulated by injecting mass into the flow and by assuming the flow was no longer isoenergetic. In other words, the enthalpy downstream of the engines was no longer assumed to be constant. The actual engine operating conditions for the Mach 2 aircraft obtained from NASA and used in the computation were as follows:

$$\rho_j/\rho_\infty = 0.4796$$

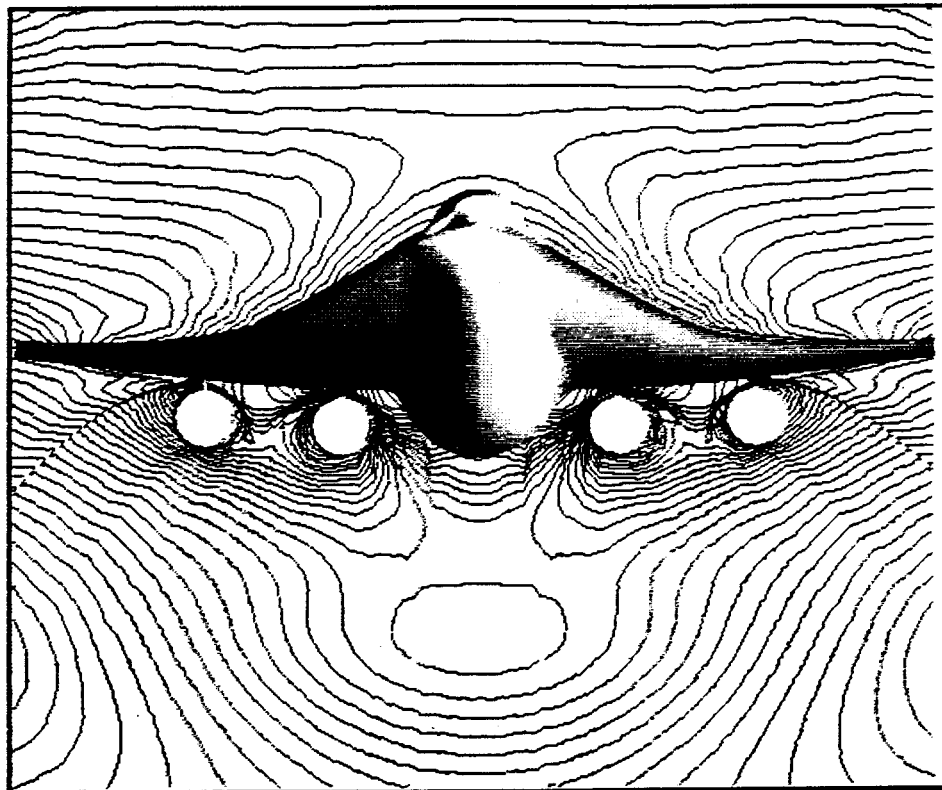
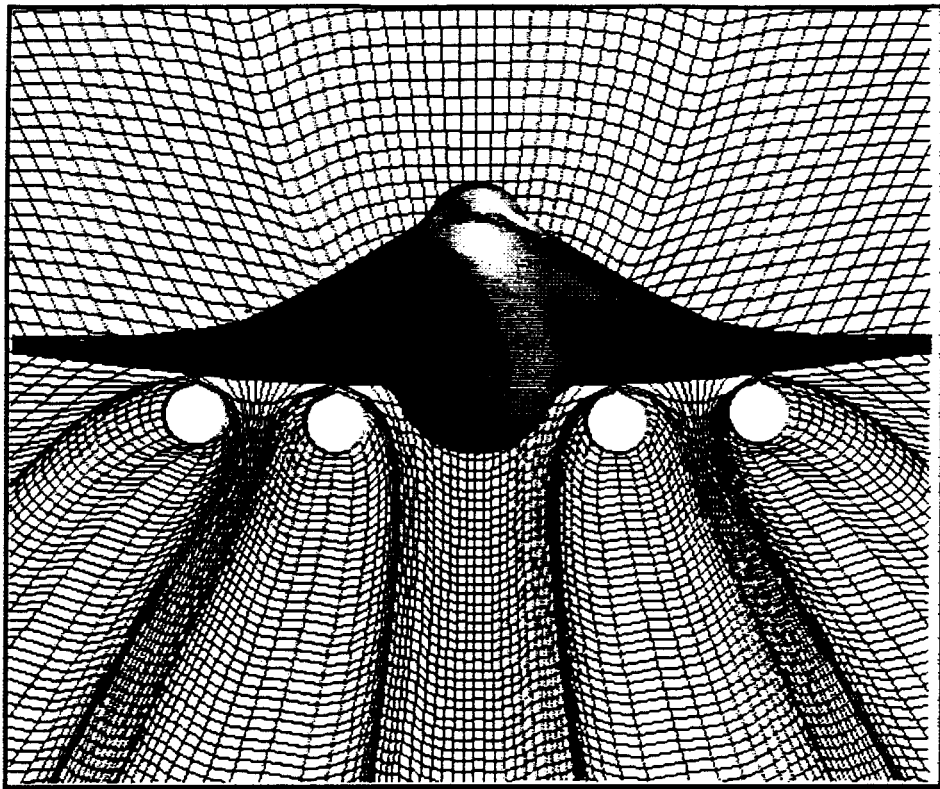
$$V_j/V_\infty = 1.697$$

$$P_j/P_\infty = 1.0$$

The exhaust pressure ratio for the Mach 2 aircraft is matched with freestream. These conditions lead to exhaust jets with approximately a 2.4 Mach number.

Due to the sparsity of mesh points within the engine exhaust itself, the details of the plume internal flow fields are not expected to be accurate. In addition, the engine exhaust mass is injected at the nearest grid points lying within the engine exit diameter. In other words, the grid does not conform to the circular exit of the nozzles and the circular geometry is only approximated within a locally Cartesian mesh.

Figure 11 shows the computational grid and computed pressure contours for the Mach 2 aircraft towards the back of the nacelles. Figure 12 shows the surface geometry of the Mach 2 concept with the engine nacelles. Figure 13 shows the simulated exhaust plumes issuing from the engine nacelles. The plumes were visualized by painting high Mach number surfaces within the flow field. In this case, Mach number surfaces greater than 2.15 Mach number were painted from the flow field.



92-0161-010

Figure 11. Grid and pressure contours toward the back of nacelles for the Mach 2 aircraft.

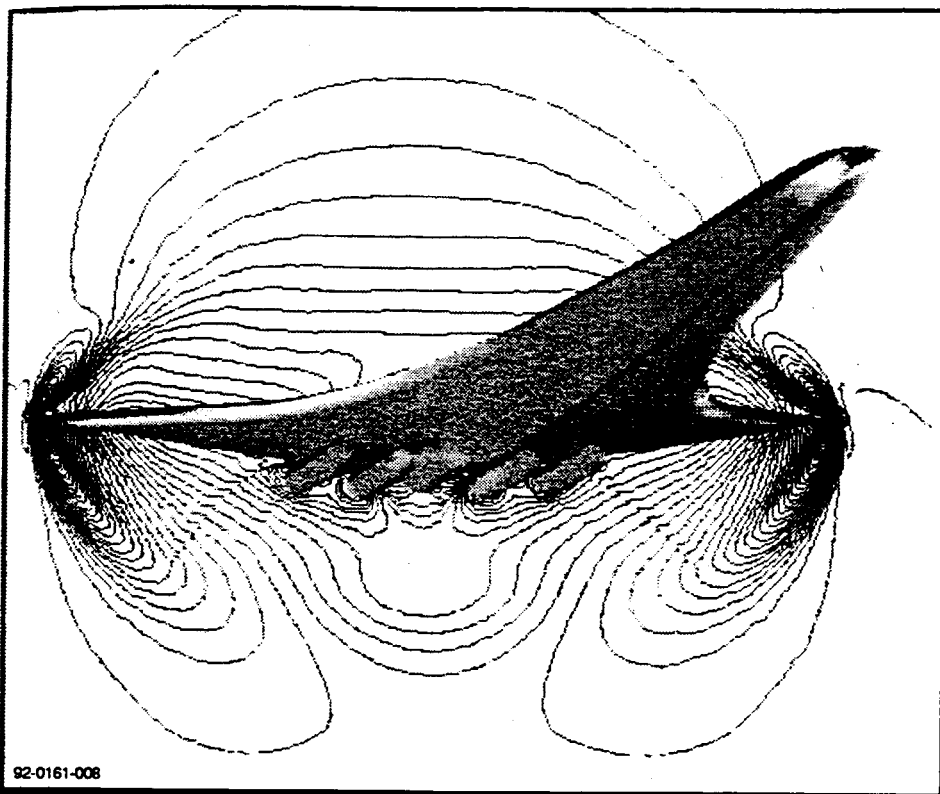


Figure 12. Surface geometry with nacelles and pressure contours for the Mach 2 aircraft.

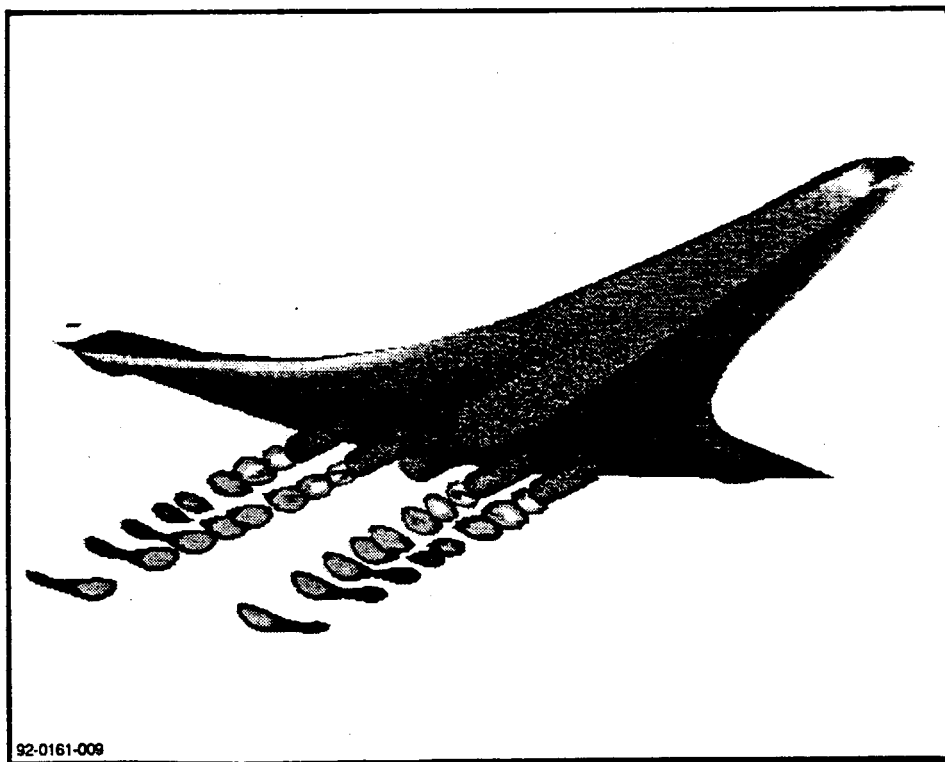


Figure 13. Pressure painted surface and high Mach surfaces in jet exhaust for the Mach 2 aircraft.

Given the above exhaust conditions with matched pressure ratio, it is not expected that a strong air shock or plume shock should develop due to a single jet exhaust. The plume air shock is typically generated by the coflow of air over the expanded plume boundary (i.e., for underexpanded jets). The combined effect of four engines in close proximity may lead to an amplification effect due to the interaction of all four plume air shocks with the sting shock and aircraft flow field. Figure 14 shows the pressure contours at stations aft of the engine exit plane. A shock is seen to develop below the engines that coalesces into a single shock extending to the lower symmetry plane of the aircraft.

The engine nacelles and exhaust simulation was also carried out for the Mach 3 aircraft using a similar block structure and number of grid points. The Mach 3 engine operating conditions were as follows:

$$\rho_J/\rho_\infty = 0.3904$$

$$V_J/V_\infty = 2.686$$

$$P_J/P_\infty = 1.048$$

The jet plume is slightly underexpanded and the jet exit Mach number for these conditions was computed as 4.92. As a result of these conditions (i.e., underexpanded jet and higher exhaust Mach number), it is expected that the engine exhaust for the Mach 3 aircraft will have a greater effect on the pressure field below the aircraft.

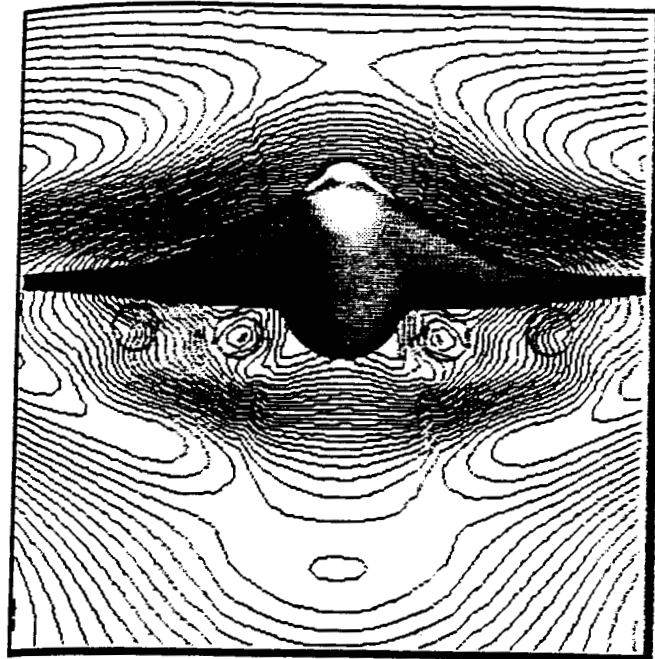
Figures 15 and 16 show the computational grid and pressure contours toward the back of the nacelles for the Mach 3 concept. The engines of the Mach 3 aircraft are not situated as close to the aircraft in comparison to the Mach 2 concept.

Figure 17 shows the exhaust simulation for the Mach 3 aircraft. The exhaust is depicted by painted surfaces with Mach number greater than 3.1. This yields some high Mach number surfaces on the leeward side of the aircraft. It is interesting to note that the aircraft flow field has a marked effect on the characteristics of the exhaust flow.

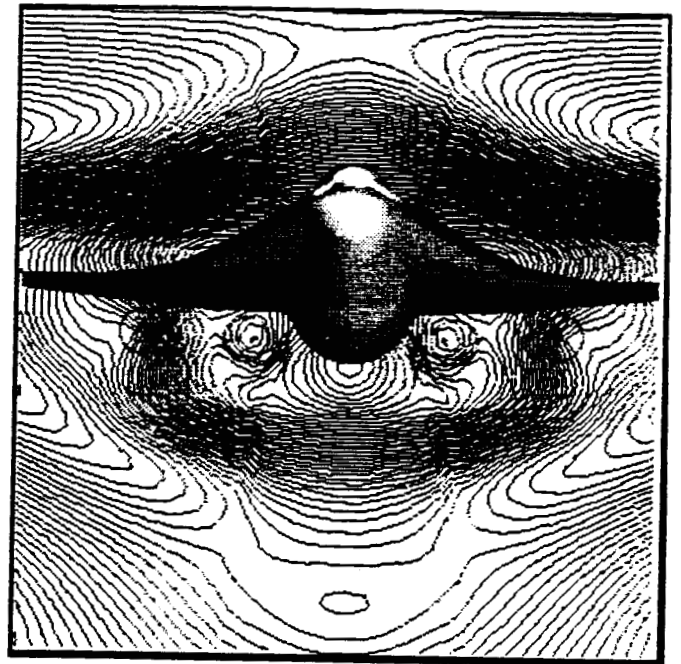
Figure 18 shows pressure contour plots at stations aft of the nacelle exit plane. For the Mach 3 aircraft a relatively strong shock quickly develops and surrounds all four nacelles. Further aft, a very complicated shock pattern develops as a result of the interaction of all four nacelles. The plume air external shocks also interact with the body sting shock. The shock system eventually moves away from the underside of the vehicle as a single strong shock in the vicinity of the symmetry plane with weaker shocks to the side.

Figure 19 shows the computed pressure footprint and signatures for the Mach 2 aircraft at one body length below the aircraft with nacelles and exhaust simulation. The effect of the exhaust can be seen in the centerline signature as a weak shock. This shock did not occur in the flow-through nacelle computation of Figure 8.

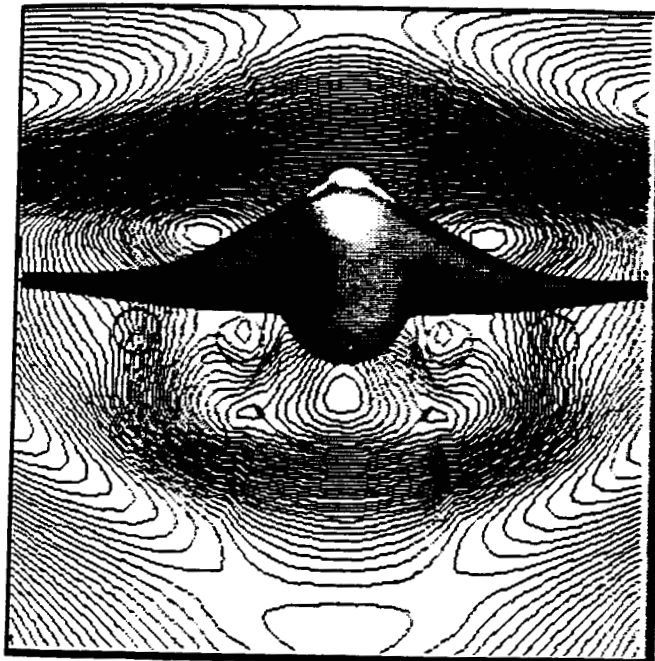
Figure 20 shows the computed pressure footprint and signatures for the Mach 3 aircraft at one body length below the aircraft with nacelles and exhaust simulation. The effect of the exhaust flow can be seen more markedly in the centerline pressure signature. The exhaust conditions of the Mach 3 aircraft lead to a much stronger shock in the signature. The engine exhaust overpressure surpasses the level of the sideline wing crank shock. Figure 20 can be compared to Figure 9 with flow-through nacelles. The effect of the engine exhaust is localized to the vicinity of the symmetry plane. The extent of this shock can be seen in the three-dimensional pressure pattern.



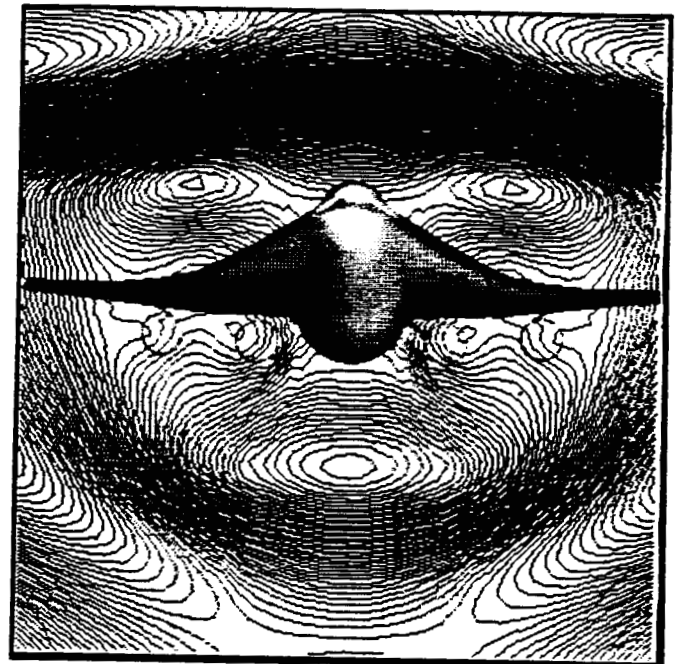
(1)



(2)



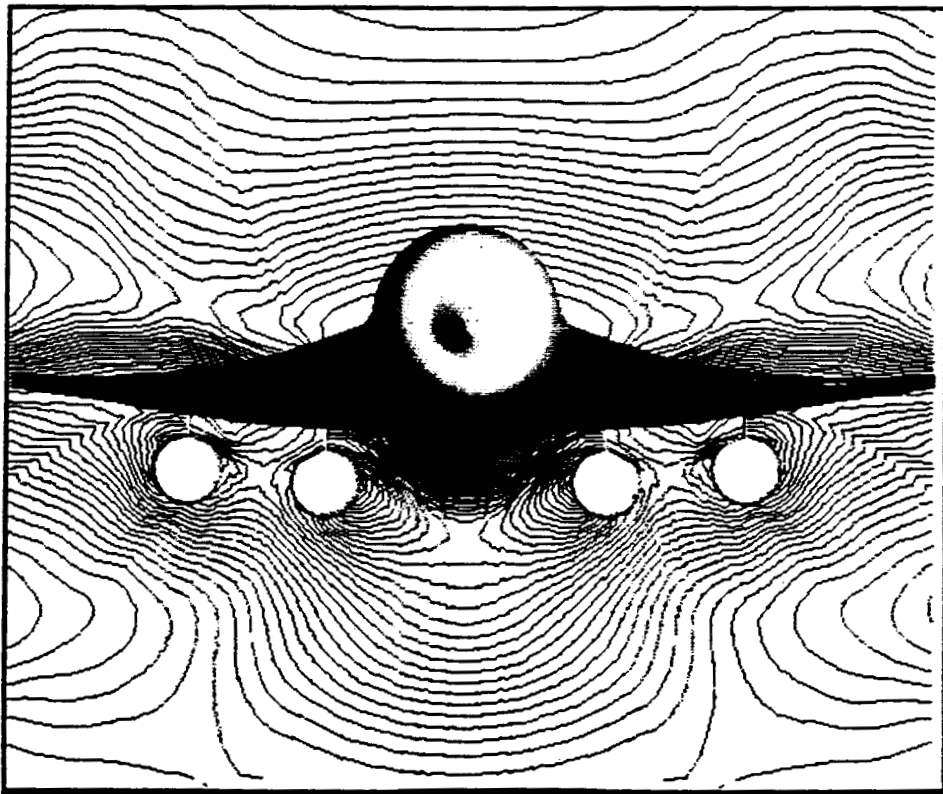
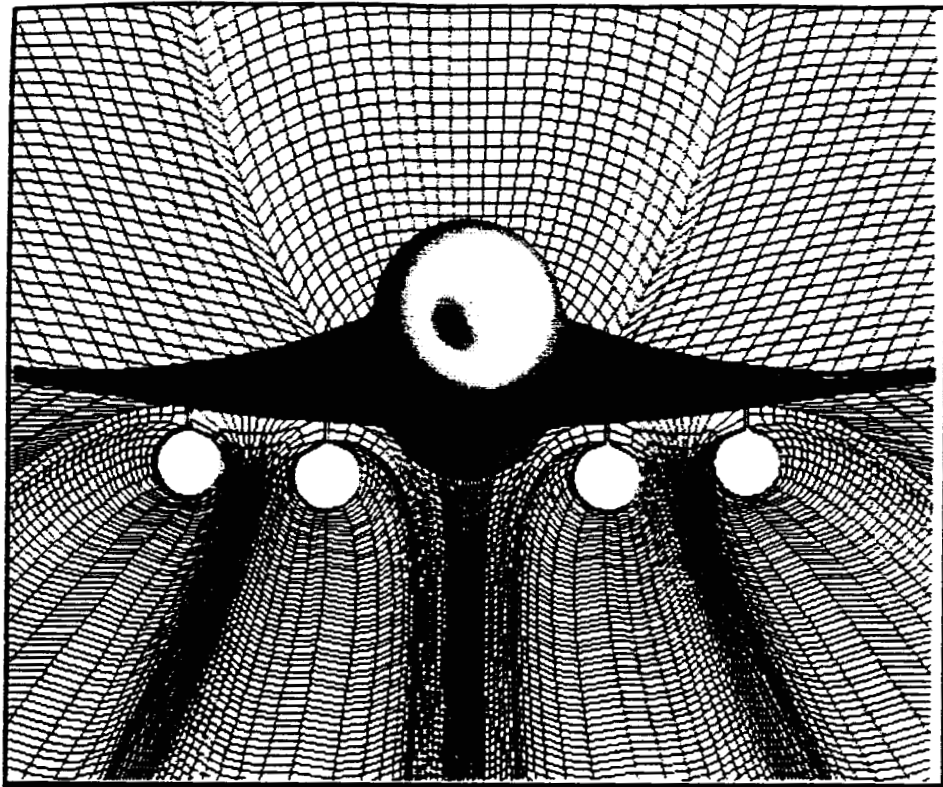
(3)



(4)

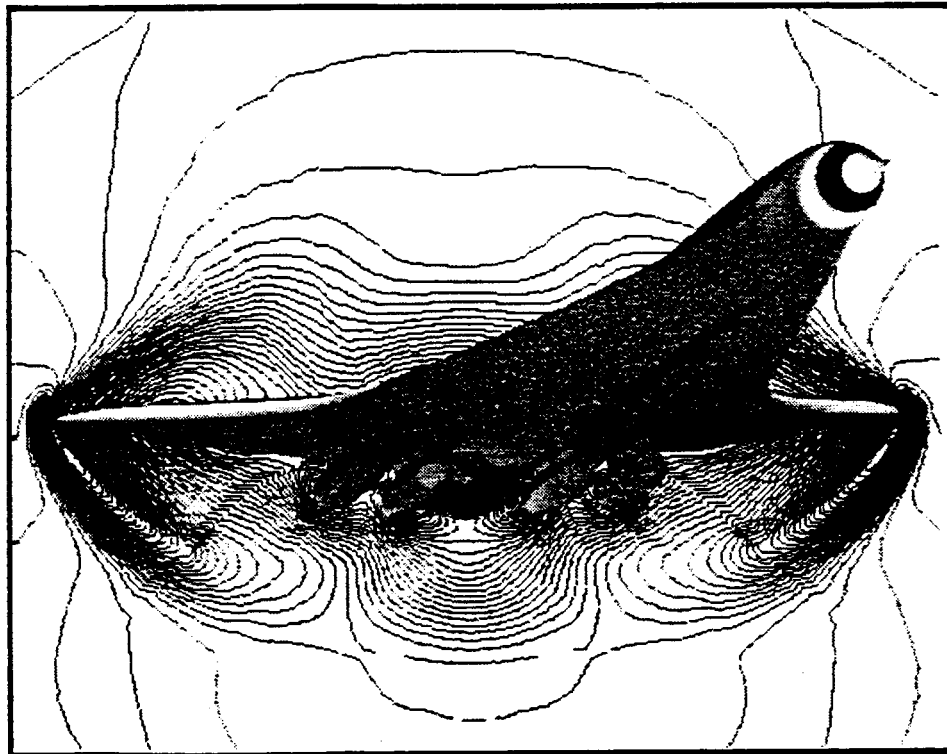
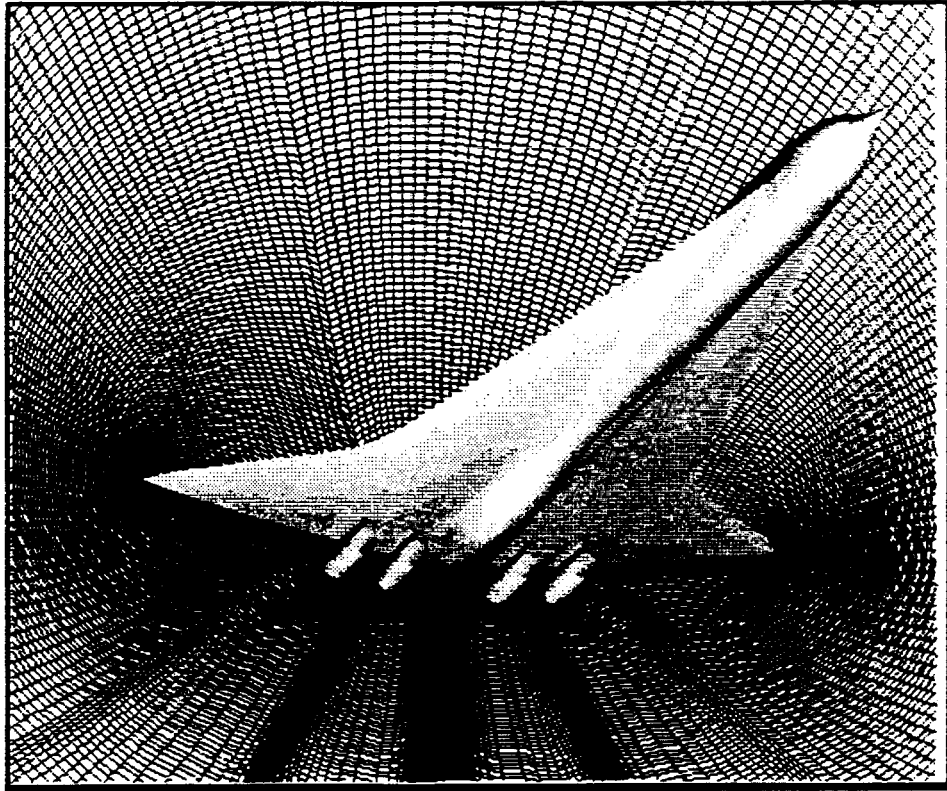
92-0161-007

Figure 14. Pressure contours downstream of nacelles with engines operating for the Mach 2 aircraft.



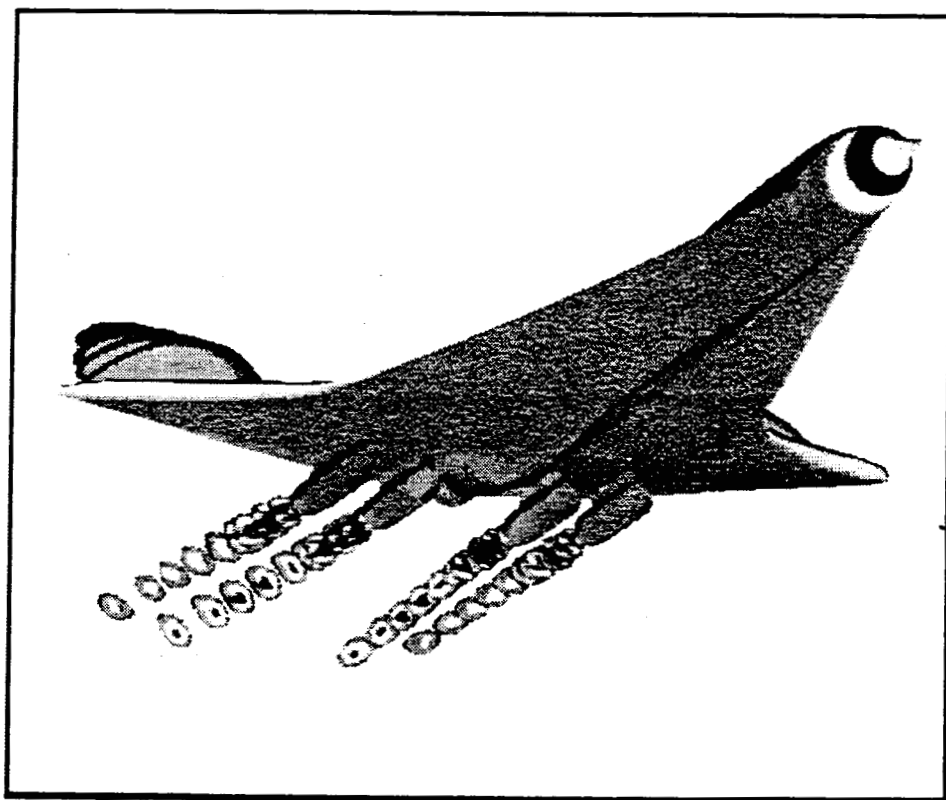
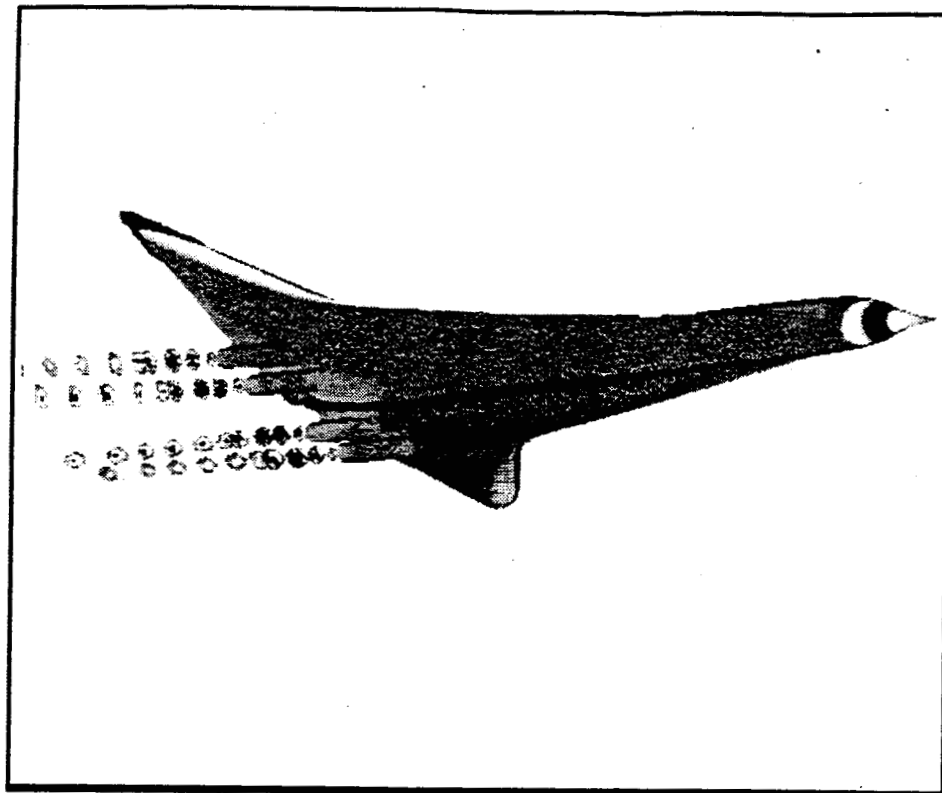
92-0161-006

Figure 15. Grid and pressure contours toward the back of nacelles for the Mach 3 aircraft.



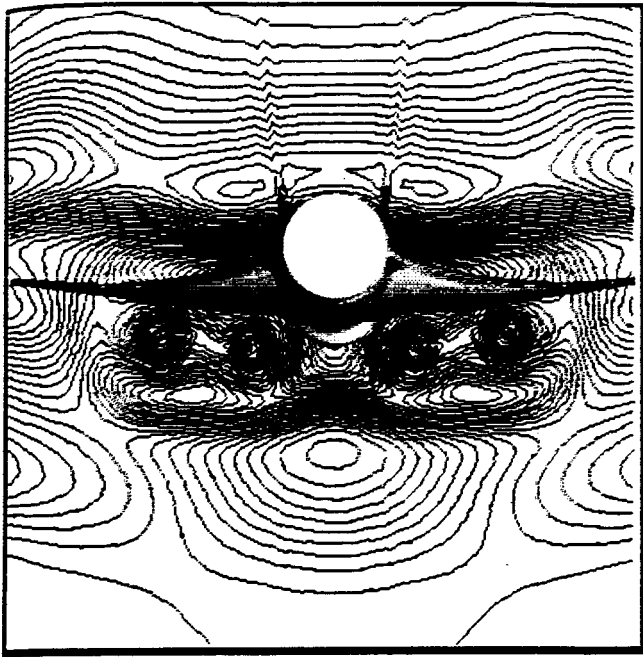
92-0161-003

Figure 16. Surface geometry with nacelles and pressure contours for the Mach 3 aircraft.

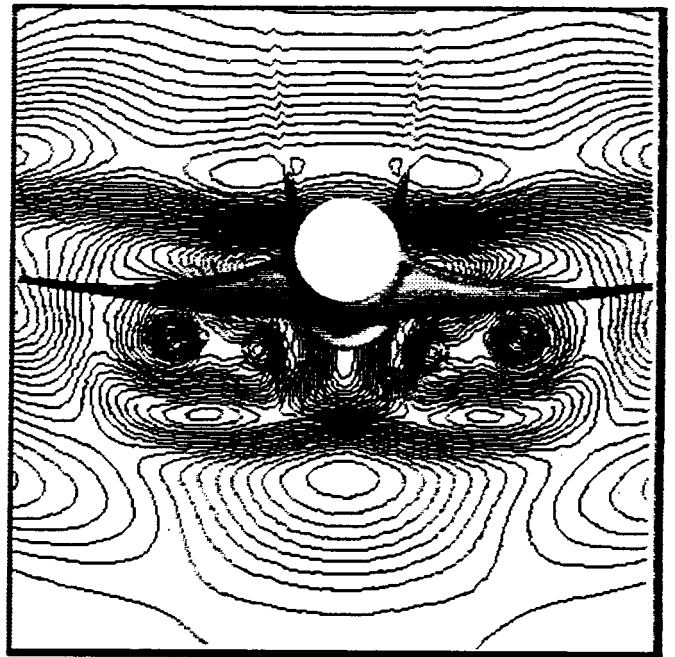


92-0161-004

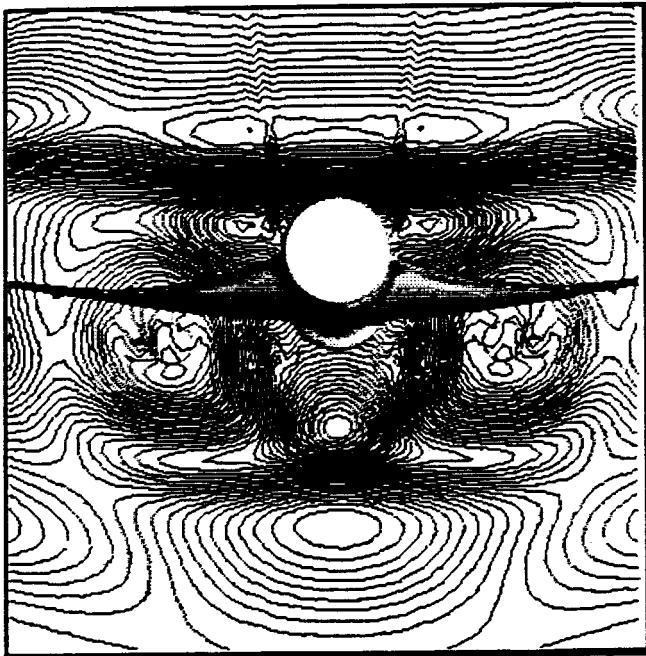
Figure 17. Pressure painted surface and high Mach surfaces in jet exhaust for the Mach 3 aircraft.



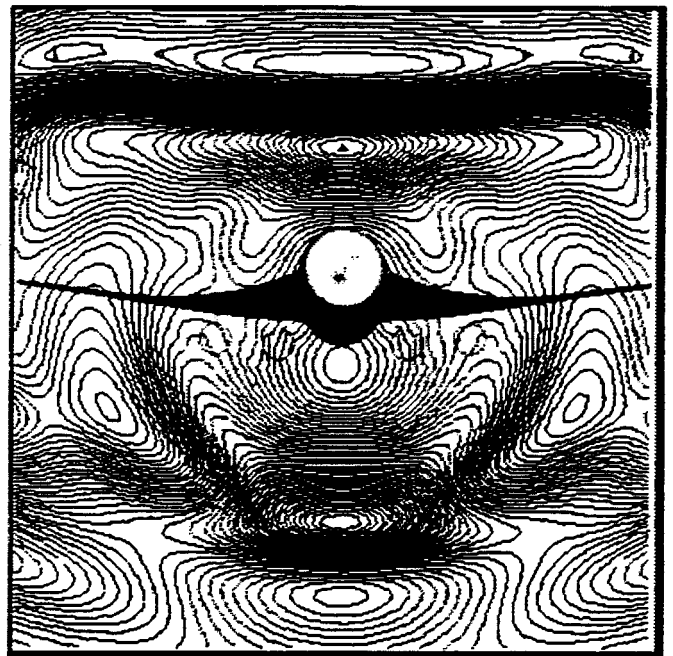
(1)



(2)



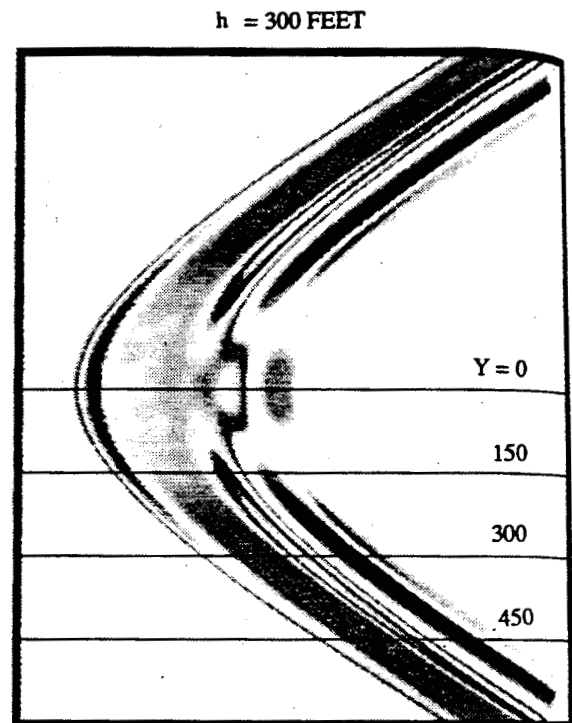
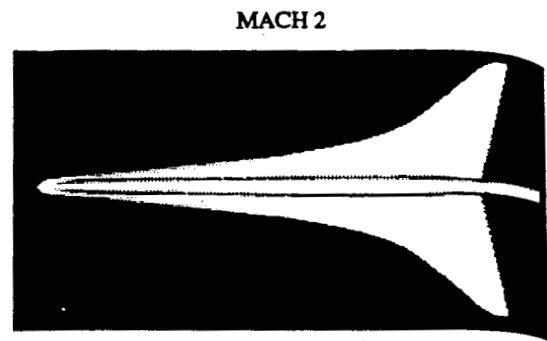
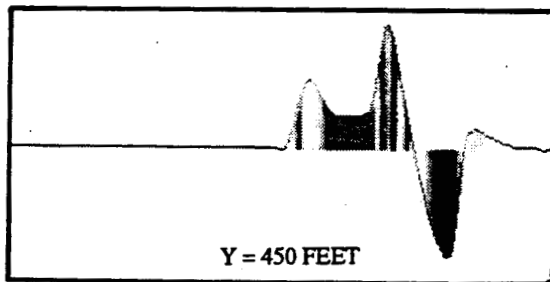
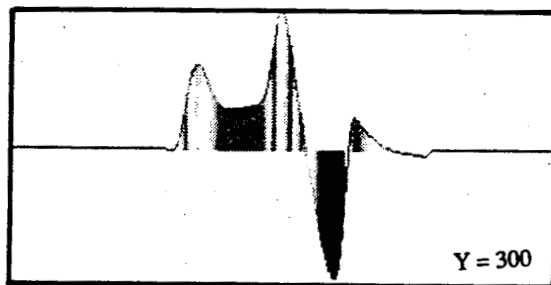
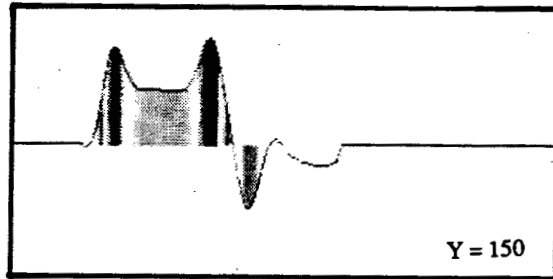
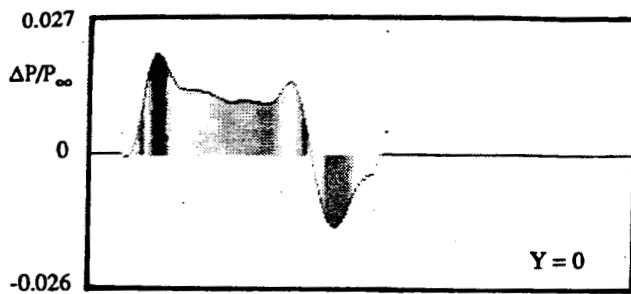
(3)



(4)

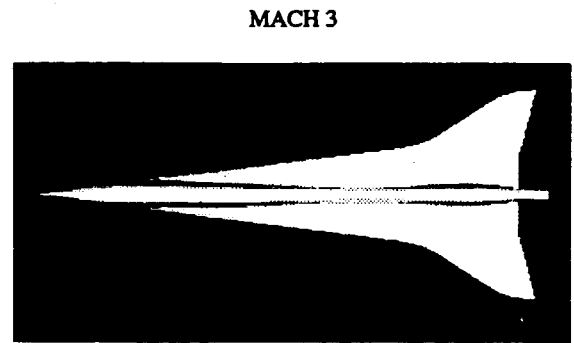
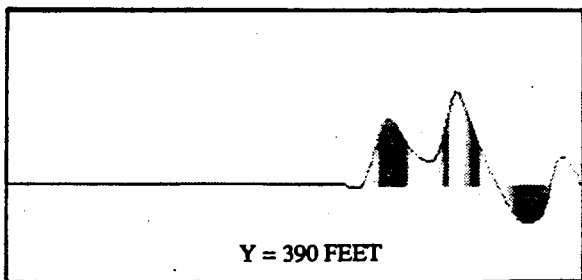
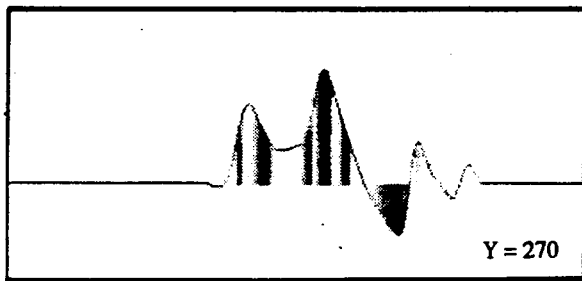
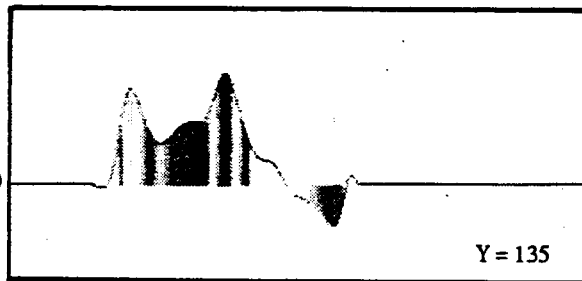
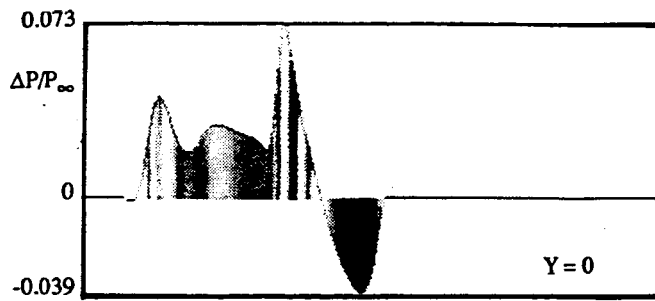
92-0161-005

Figure 18. Pressure contours downstream of nacelles with engines operating for the Mach 3 aircraft.

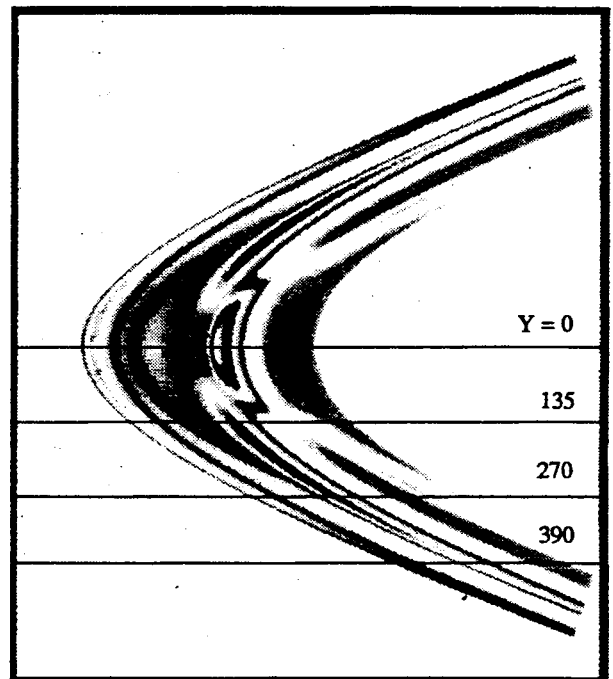


92-0161-020

Figure 19. Pressure footprint and sideline signatures at $h/l=1$ for the NASA Mach 2 low boom aircraft with engine exhaust simulation.



h = 300 FEET



92-0161-021

Figure 20. Pressure footprint and sideline signatures at $h/l=1$ for the NASA Mach 3 low boom aircraft with engine exhaust simulation.

The effect of the engine exhaust on the overall centerline signatures can be summarized by Figure 21. The solid lines represent flow-through nacelles and the dashed lines represent the effect of engines with plume exhaust simulation. The Mach 2 exhaust has only a minor effect on the near-field pressure signature but when extrapolated to the ground yields a secondary downstream shock with an overpressure magnitude slightly greater than the initial shock. However, the increment or delta is relatively small for this shock.

The Mach 3 exhaust shows a marked effect on the near-field signature in the form of a relatively strong secondary shock. When extrapolated to the ground, the shocks coalesce and the signature becomes a standard N-wave with an increase in overpressure from about 1.5 to above 2 lbs/ft².

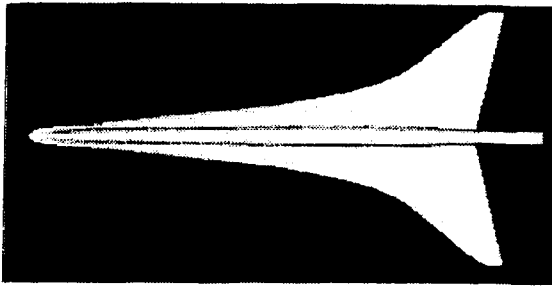
CONCLUSIONS

The present study has demonstrated that three-dimensional effects that may be neglected in standard sonic boom minimization techniques should be considered more carefully. It has been demonstrated that sideline boom overpressures can be higher than the levels occurring directly below the aircraft by as much as 25%. These higher sideline overpressures are primarily due to the cranked supersonic leading edge outboard panel of the wing. In addition to marginally accounting for three-dimensional effects, any form of linear theory may be inadequate in dealing with the class of strong shocks that occur for supersonic leading wings. These shocks violate the premise of linear theory.

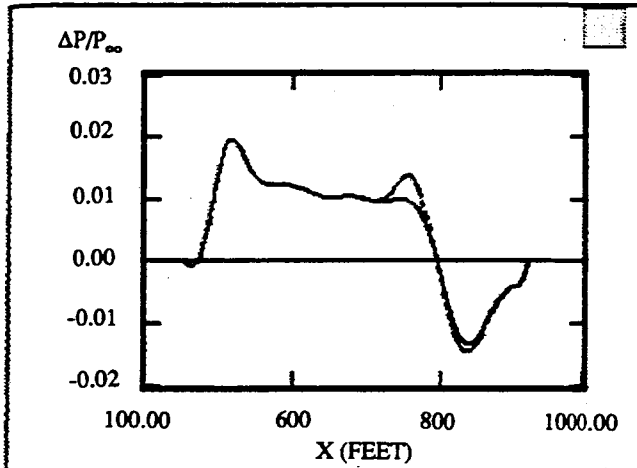
Engine effects also were studied. It was found that for the class of nacelle geometry studied (i.e., underwing nacelles hung from pylons), the effect of nacelles alone (i.e., flow-through) did not significantly alter the sonic boom signature. The engine exhausts were also simulated. It was found that the effect of the exhaust on the signature and the generation of multiple plume shock waves interacting with each other and the surrounding aircraft flow field was sensitive to the engine operating conditions. For the Mach 2 aircraft with matched pressure exhaust and lower velocity ratio, the effect of the exhaust generated a relatively weak secondary shock in the signature just prior to expansion. On the other hand, the Mach 3 concept with a slightly underexpanded operating condition and higher velocity ratio, resulted in a much stronger secondary shock in the signature which coalesced with the nose shock to form an N-wave at the ground. Hence, it increased the boom overpressure by about 15%.

A lower Mach 1.7 Boeing-911 configuration was also studied and found to yield an overpressure at the ground of about 1.5 lbs/ft². The Mach 3 configuration was designed to have a ramped type of pressure signature. The computed results for this aircraft did not yield a signature that exhibited the ramp shape of the target design signature. On the other hand, the Mach 2 and Mach 1.7 aircraft were designed for a flat topped signature. The target shape of the Mach 2 concept and overpressure levels was essentially achieved directly underneath the aircraft. On the other hand, the Boeing-911 configuration did not exhibit the target flat top shape and also exhibited higher levels than expected.

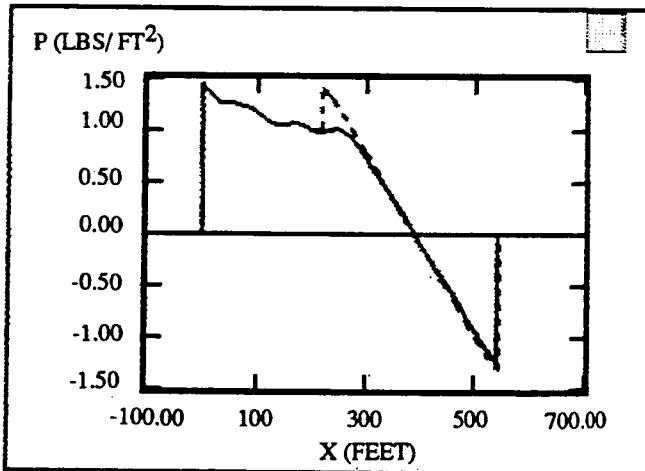
MACH 2



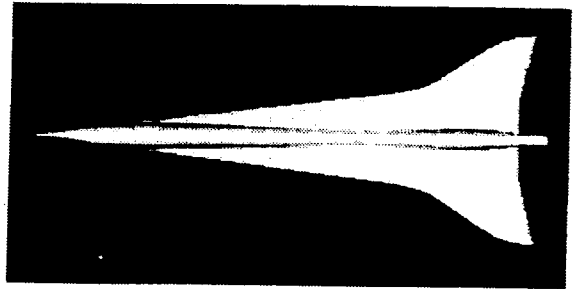
$h/l = 1$



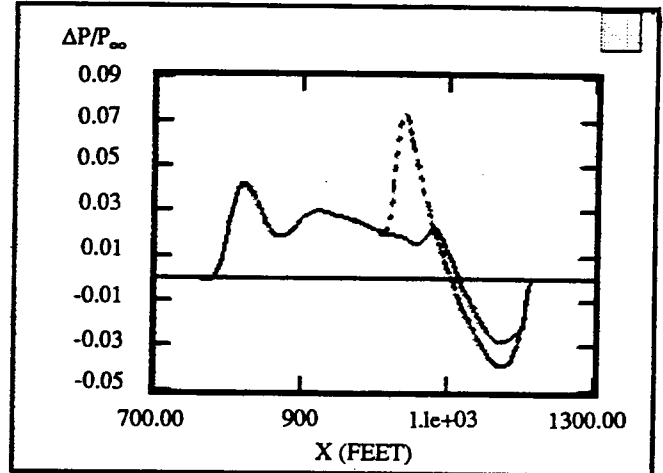
$h = 55000$ FT



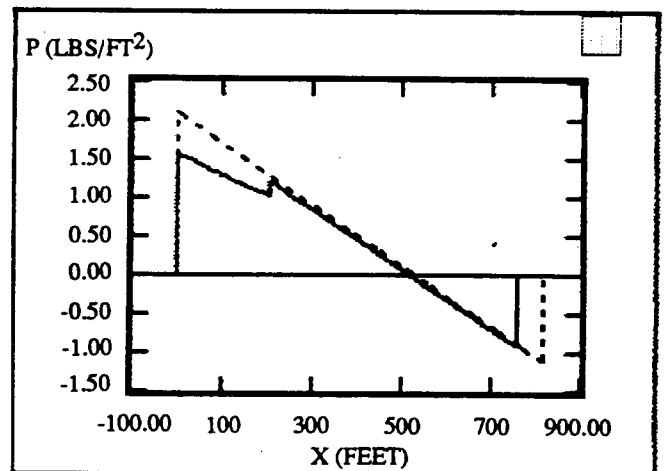
MACH 3



$h/l = 1$



$h = 65000$ FT



92-0161-002

Figure 21. Comparison of $h/l=1$ and extrapolated ground signatures for both flow-through nacelles and nacelles with engine exhaust simulation for the Mach 2 and Mach 3 configurations.

REFERENCES

1. Whitham, G.B.: The Flow Pattern of a Supersonic Projectile. *Comm. Pure & Applied Math.*
2. Walkden, F.: The Shock Pattern of a Wing-Body Combination, Far From the Flight Path. *Aeronautical Q.*, vol. IX, pt. 2, May 1958, pp. 164-194.
3. Siclari, M. J. and Darden, C.: CFD Predictions of the Near-Field Sonic Boom Environment for Two Low Boom HSCT Configurations. AIAA Paper No. 91-1631, presented at AIAA 22nd Fluid Dynamics, Plasma Dynamics & Lasers Conference, Honolulu, HI, June 1991.
4. Thomas, C. L.: Extrapolation of Sonic Boom Pressure Signatures by the Waveform Parameter Method. NASA TN D-6832, 1972.
5. Siclari, M. J. and Del Giudice, P.: Hybrid Finite Volume Approach to Euler Solutions for Supersonic Flows. *AIAA J.*, vol. 28, no. 1, Jan. 1990, pp. 66-74.
6. Siclari, M. J.: Three-Dimensional Hybrid Finite Volume Solutions to the Euler Equations for Supersonic/Hypersonic Aircraft. AIAA Paper No. 89-0281, presented at AIAA 27th Aerospace Sciences Meeting, Reno, NV, Jan. 1989.
7. Mack, R. J. and Needleman, K. E.: The Design of Two Sonic Boom Wind Tunnel Models from Conceptual Aircraft which Cruise at Mach Numbers of 2.0 and 3.0. AIAA Paper No. 90-4026, presented at AIAA 13th Aeroacoustics Conference, Tallahassee, FL, Oct. 1990.